Asian Journal of
Science, Technology, Engineering, and Art

e-ISSN: 3025-4507
p-ISSN: 3025-5287
Index: Harvard, Boston, Sydney University, Dimensions, Lens, Scilit, Semantic, Google, etc

https://doi.org/10.58578/AJSTEA.v4i2.9188

Thermal Transport Characteristics of Fractional Maxwell Fluid Model for Blood Flow in a Stenosed Artery

Ali Musa[1], A. M Kwami[2], A. G Madaki[3]
[1]Yobe State University Damaturu, Nigeria
[2,3]Abubakar Tafawa Balewa University, Bauchi, Nigeria
isahabdullahi7474@gmail.com

Article Info:

Submitted:	Revised:	Accepted:	Published:
Feb 8, 2026	Mar 8, 2026	Mar 20, 2026	Mar 25, 2026

Abstract

This study examines the unsteady heat transfer behavior of fractional Maxwell nanofluid blood flow in a stenosed artery under the combined effects of a magnetic field, thermal radiation, viscous dissipation, and internal heat generation. The study aims to provide a more realistic representation of thermal transport in pathological blood flow by incorporating fractional-order viscoelastic effects. The governing fractional energy equation is solved using a semi-analytical Laplace transform approach, while numerical inversion is carried out through the Concentrated Matrix-Exponential method. The results show excellent agreement with existing studies, confirming the validity of the proposed approach. The findings further reveal that thermal radiation, magnetic field strength, viscous dissipation, fractional order, and relaxation time increase temperature distribution, whereas higher Reynolds and Prandtl numbers reduce it. The study concludes that fractional-order modeling offers a more realistic and effective framework for analyzing thermal transport in stenosed arterial blood flow, thereby contributing to improved understanding of heat transfer behavior in pathological hemodynamic conditions.

AJSTEA Journal is licensed under a Creative Commons Attribution-NonCommercial-ShareAlike 4.0 International License

Keywords: Fractional Maxwell Nanofluid; Stenosed Artery; Heat Transfer; Thermal Radiation; Magnetic Field

Introduction

Cardiovascular diseases remain one of the leading causes of mortality worldwide, with arterial stenosis playing a critical role in the development of pathological blood flow conditions. Stenosis, characterized by the narrowing of arterial passages, significantly alters hemodynamic behavior, leading to abnormal velocity distributions, enhanced wall shear stress, and thermal variations within the arterial system. The pioneering experimental investigation of pulsatile flow in constricted tubes by Ahmed and Giddens (1983) established the fundamental hydrodynamic consequences of arterial narrowing, providing a foundation for subsequent analytical and computational studies.

Blood exhibits complex rheological characteristics, particularly under low shear rates encountered in small or diseased arteries. Although early studies modeled blood as a Newtonian fluid, modern investigations confirm its non-Newtonian and viscoelastic behavior. For instance, Kot and Elmabound (2021) applied fractional calculus to analyze pulsatile blood flow in stenosed arteries, demonstrating that fractional-order models provide improved accuracy compared to classical integer-order approaches. Similarly, Jamil et al. (2021) investigated magnetic Casson blood flow in inclined stenosed arteries using Caputo–Fabrizio fractional derivatives, revealing that fractional modeling effectively captures memory-dependent flow characteristics.

The influence of magnetic fields on blood flow has attracted considerable attention due to its applications in magnetic drug targeting, hyperthermia treatment, and biomedical diagnostics. Adamu et al. (2020) studied magnetohydrodynamic (MHD) blood flow through stenosed arteries under inclined magnetic fields, showing that Lorentz forces significantly suppress velocity profiles. More recently, Wang et al. (2022) numerically examined pulsatile non-Newtonian blood flow with heat transfer in small vessels subjected to magnetic fields, reporting that magnetic intensity strongly modifies both velocity and temperature distributions. Furthermore, Yakubu et al. (2025) extended MHD modeling to ternary nanofluids in inclined arteries, emphasizing the combined effects of magnetic fields and thermal radiation.

Thermal transport within blood flow is equally important, particularly in therapeutic procedures involving localized heating. Chamkha and BenNakhi (2008) investigated MHD mixed convection with radiation effects, while Hayat et al. (2017) incorporated advanced heat flux models to account for non-Fourier thermal behavior. Ghasemi et al. (2011) and Khanafer et al. (2003) demonstrated that nanofluids significantly enhance heat transfer due to improved thermal conductivity and Brownian motion effects. In biomedical contexts, Ellahi et al. (2019) analyzed peristaltic blood flow containing nanoparticles under chemical reaction and activation energy effects, highlighting the importance of nanoparticle-induced thermal enhancement.

The inclusion of nanoparticles in blood flow models has opened new research directions in targeted drug delivery and enhanced thermal regulation. Sheikholeslami (2018) examined Lorentz force effects on nanofluid flow in porous geometries, showing that magnetic fields alter nanoparticle transport behavior. Hussain et al. (2019) and Mahanthesh et al. (2017) further demonstrated that hybrid nanofluids significantly modify thermal and flow characteristics in porous and radiative environments.

In recent years, fractional calculus has emerged as a powerful tool for modeling complex transport phenomena. Han et al. (2022) proposed high-precision numerical schemes for fractional diffusion systems, while Che et al. (2022) showed that fractional derivatives reveal novel spatiotemporal dynamics in reaction–diffusion models. In the context of biofluid mechanics, Alhachami et al. (2024) confirmed that time-fractional magnetohydrodynamic models provide more realistic descriptions of viscous fluid flow compared to classical formulations. Nazar and Shabbir (2023) further emphasized the importance of fractional derivatives in analyzing irreversibility in nanofluid flow through inclined arteries.

Despite these significant contributions, most existing studies either focus on velocity characteristics or consider thermal transport without fully incorporating fractional viscoelastic memory, magnetic field effects, viscous dissipation, and internal heat generation simultaneously in stenosed arterial geometries. Moreover, numerical inversion techniques for fractional Laplace-domain solutions remain computationally challenging. Horváth (2019) introduced the Concentrated Matrix-Exponential (CME) method, which offers superior stability and accuracy for numerical inversion of Laplace transforms, making it particularly suitable for fractional-order biofluid problems.

Although numerous investigations have been conducted on magnetohydrodynamic blood flow, nanofluid heat transfer, and fractional viscoelastic modeling, most existing studies treat these mechanisms either independently or in partially coupled forms. Classical integer-order models often fail to capture the hereditary and memory-dependent characteristics of blood rheology, particularly under pathological conditions such as arterial stenosis where low shear rates and viscoelastic effects become dominant. While studies such as Kot and Elmabound (2021) and Jamil et al. (2021) demonstrated the effectiveness of fractional derivatives in modeling non-Newtonian blood flow, the combined thermal effects of magnetic fields, radiation, viscous dissipation, and internal heat generation within a fractional Maxwell framework remain insufficiently explored.

Furthermore, the increasing application of magnetic nanoparticles in biomedical engineering, particularly in hyperthermia treatment and targeted drug delivery, necessitates a more realistic thermal transport model that accounts for magnetically induced forces and nanoparticle-enhanced conductivity. Previous studies, including Wang et al. (2022) and Yakubu et al. (2025), emphasized the influence of magnetic fields and radiation on nanofluid blood flow; however, the integration of fractional-time dynamics with detailed thermal mechanisms in stenosed arterial geometries is still limited. In addition, solving fractional-order governing equations in the Laplace domain presents computational challenges, particularly when modified Bessel functions arise in cylindrical geometries. Therefore, there is a strong need for a stable and accurate numerical inversion technique capable of handling such complexities.

The motivation of this study arises from these identified gaps. Specifically, there is a necessity to develop a comprehensive fractional Maxwell nanofluid model that simultaneously incorporates magnetic field effects, thermal radiation, viscous dissipation, internal heat generation, and stenosed arterial geometry, while employing a robust numerical approach to ensure computational stability and accuracy. Such an integrated framework is essential for achieving more realistic predictions of thermal transport behavior in pathological blood flow conditions.

The primary aim of this study is to develop and analyze a comprehensive fractional-order mathematical model that accurately describes the thermal transport characteristics of Maxwell nanofluid blood flow in a stenosed artery under the combined influence of magnetic field, thermal radiation, viscous dissipation, and internal heat generation. The study seeks to

incorporate the Caputo fractional derivative into the governing energy equation in order to capture the memory-dependent viscoelastic behavior of blood, which cannot be adequately represented using classical integer-order formulations.

Methodology

Formulation of Problem

In this study, we examine the behavior of a compressible, axially symmetric, unsteady blood flow within a stenosed artery, accounting for complex physiological and physical effects. The artery is modeled as a cylindrical tube with an axisymmetric stenosis (narrowing), which is a common pathological condition in cardiovascular systems. To simulate realistic biomedical conditions, blood is treated as a non-Newtonian viscoelastic fluid using a fractional Maxwell model. This choice reflects the complex rheological behavior of blood, especially under low shear rates found in small or stenosed arteries. In addition to its inherent viscoelastic nature, the blood is considered to carry suspended nanoparticles (e.g., copper, gold, or aluminum oxide), enhancing its thermal and mass transport properties. The geometric parameters defining the artery include r: the radial coordinate,

z: the axial coordinate along the artery's length, and R(z): the stenosis shape function defining local reduction in radius. The collective influence of these parameters on the dynamics of fluid flow is illustrated in Figure 1.

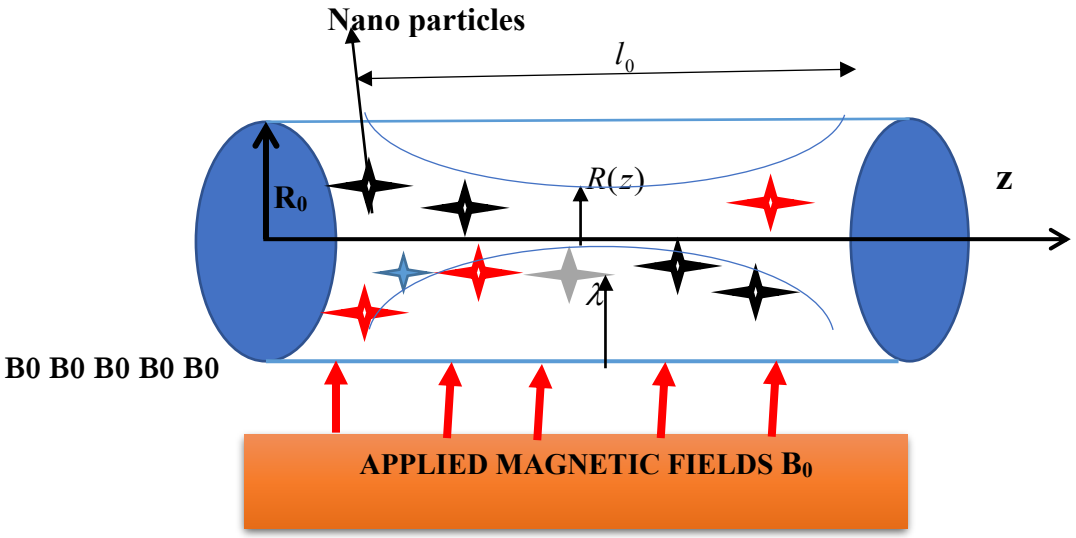


Figure 1a: Flow Geometry of the Stenosed Artery

The geometry of the stenosed region is specified using a shape function $R(z)$, as described in Equation (10) of Section 2.2. This function defines the varying arterial radius along the axial direction, characterized by maximum stenosis height λ and stenosis length l_0. An external transverse magnetic field B_0 is applied perpendicular to the flow direction. The magnetic field interacts with the electrically conducting blood to produce a Lorentz force, which resists the motion and modifies velocity profiles.

The Energy Equation

The mathematical formulation governing the blood flow of the consists of a nonlinear, fractional partial differential equations that describe the Energy equation as referenced in (Wang et al., 2022, and Yakubu et al.,2025) is given by:

$$\rho C_{\rho} \frac{\partial \overline{T}}{\partial \bar{t}} = k_T \frac{\partial}{\partial r}(r \frac{\partial \overline{T}}{\partial \bar{r}}) - \frac{\partial \overline{q}}{\partial \bar{r}} + Q(T - T_0\bar{)} + \sigma B_0^2 \bar{u}^2 + \mu(\frac{\partial u}{\partial r})^2 \quad (1)$$

Where

$$-\frac{\partial q}{\partial \bar{r}} = 4\alpha^2\left(\overline{T} - \overline{T}_0\right) \quad (2)$$

Is the thermal radiation within a vibrational environment,

The symbols $\rho, \bar{t}, \bar{r}, \bar{p}, \mu, , \overline{T}, \overline{T}_{0,}, C_p, Q, k_{T,} B_0, \bar{u},$ have been properly defined in Table 1.

Table 1. Nomenclature

Symbol	Description	Unit
C_p	Specific heat capacity	$jkg^{-1}K^{-1}$
θ	Dimensionless temperature	K^{-1}
ρ	Density	kg/m^3
μ	Dynamic viscosity	Pas
B_0	Magnetic field	T
r	Radial Coordinate	m
a_0, a_1	Stenosis amplitude parameter	_
T_0	Free stream temperature	K^{-1}
u	Blood Velocity	m/s
Q	Amount of heat	$Joule$
T	Wall temperature	K^{-1}

The above equation is governed by the corresponding initial and boundary conditions.

$$\left.\begin{array}{llll} \bar{u}=\bar{u}_0, \bar{T}=\bar{T}_0, \forall \bar{r} \in (0.R_0), & at & \bar{t}=0 & \\ \dfrac{\partial \bar{u}}{\partial \bar{r}}=0, \dfrac{\partial \bar{T}}{\partial \bar{r}}=0,; & \forall t>0, & at & \bar{r}=0 \\ \bar{u}=0, \bar{T}=\bar{T}_w, \ \forall \bar{t}>0 & at & & \bar{r}=\bar{R}(\bar{z}) \end{array}\right\} \quad (3)$$

The symbols $\bar{u}_0, \bar{T}_0$ maintained their usual meaning, and $\bar{R}(\bar{z})$ represent the equation that models the stenosed region, as stated in (Imoro et al.,2024) as follows:

$$\bar{R}(\bar{z})=\begin{cases} R_0-\dfrac{\lambda}{2}\left(1+\cos\left(\dfrac{4\pi\bar{z}}{l_0}\right)\right), -\dfrac{l_0}{4}<\bar{z}<\dfrac{l_0}{4} \\ R_0, \quad otherwise \end{cases} \quad (4)$$

The symbols l_0 and λ represent the length of the artery and the maximum height of the stenosis, respectively.

These governing equations are supplemented by appropriate initial and boundary conditions reflecting physiological constraints, such as no-slip velocity at the artery wall, specified wall temperature and concentration, and symmetry conditions along the artery centerline.

Solution technique

By employing the following parameters, equation (1)-(4) for can be rendered dimensionless;

$$\left.\begin{array}{l} r=\dfrac{\bar{r}}{R_0}, z=\dfrac{\bar{z}}{R_0}, t=\dfrac{u_0\bar{t}}{R_0}, u=\dfrac{\bar{u}}{u_0}, p=\dfrac{\bar{p}}{\rho u_0^2}, R(z)=\dfrac{\bar{R}(\bar{z})}{R_0} \\ \theta=\dfrac{\bar{T}-T_0}{T_0-T_\infty}, Q_s=\dfrac{R_0\bar{Q}_s}{u_0\rho\bar{C}p(T-T_0)}, \end{array}\right\} \quad (5)$$

By applying eqns. (5) into eqns. (1-4) and dropping the bars, we have:

$$P_e\frac{\partial\theta}{\partial t}=\frac{\partial^2\theta}{\partial r^2}+\frac{1}{r}\frac{\partial\theta}{\partial r}+(Ra+P_eQ_s)\theta(r,s)+Ha^2Bru^2+Br\left(\frac{\partial u}{\partial r}\right)^2 \quad (6)$$

$$\left.\begin{array}{llll} u=u_{z0}, \theta=\theta_0, & \forall r\in(0,1), & at & t=0 \\ \dfrac{\partial u}{\partial r}=0, \dfrac{\partial\theta}{\partial r}=0, & \forall t>0, at & & r=0 \\ u_z=\vartheta,, \theta=\theta_w, & \forall t>0, & at & r=R(z) \end{array}\right\} \quad (7)$$

Where ϑ represents the drag velocity along arterial walls whilst $R(z)$ is the dimensionless form of Equation (10), expressed as follows:

$$R(z)=\begin{cases}1-\dfrac{\lambda}{2R_0}\left(1+\cos\left(\dfrac{4\pi z R_0}{l_0}\right)\right), & -\dfrac{l_0}{4R_0}<z<\dfrac{l_0}{4R_0}\\ 1, & otherwise\end{cases} \tag{8}$$

Where

$$Ha^2=\frac{\sigma_f B_0^2 R_0}{\mu_f},\Pr=\frac{\mu_f C_p}{k_f},Q_s=\frac{QR_0^2}{k_T},Br=Ec\,\Pr,$$

$$\mathrm{Re}=\frac{R_0 u_{z0}}{v},,Ra=\frac{4\alpha_1^2 R_0^2}{k},Pe=\mathrm{Re}.\Pr,Ec=\frac{u_{z0}^2}{C_p(T_0-T_\infty)}$$

are defined as Hartman Number, Prandtl number, Heat source parameter,Brickman number, Reynolds number, thermal radiation parameter, and Eckert number respectively.

Fractional-Time Derivatives of Modeled Equations

Fractional-order models provide improved precision in representing spatial diffusion and memory effects, making them particularly well-suited for complex biological systems. Advanced numerical techniques for space-fractional models, such as those proposed by Han et al., (2022), have demonstrated high effectiveness in accurately describing diffusion processes, enhancing the stability of fractional differential equations, and offering reliable tools for simulating intricate biological phenomena. The incorporation of Riesz fractional derivatives in reaction–diffusion models, as shown by Che et al., (2022) uncovers novel spatiotemporal behaviors, enhances the accuracy of anomalous transport analysis, and delivers a more generalized framework for biofluid dynamics. Furthermore, the application of fractional calculus in modeling non-Newtonian blood flow is supported by works such as Jamil et al., (2021) who utilized Caputo–Fabrizio fractional derivatives to study magnetic Casson blood flow in inclined stenosed arteries. Likewise, Alhachami et al., (2023) examined time-fractional magnetohydrodynamic flow over a plate, further confirming the effectiveness of fractional derivatives in blood flow analysis. Collectively, these studies highlight the relevance of fractional-time derivatives for capturing the complex dynamics of biological fluids. Accordingly, by introducing the Caputo fractional derivative into the transient terms of Equation (6), we obtain

$$P_e D_t^{\alpha}\theta=\frac{\partial^2\theta}{\partial r^2}+\frac{1}{r}\frac{\partial\theta}{\partial r}+(Ra+P_eQ_s)\theta(r,s)+Ha^2Bru^2+Br\left(\frac{\partial u}{\partial r}\right)^2 \tag{9}$$

where

$$t_0^{1-\alpha} D_t^{\alpha} u(r,t) = \frac{t_0^{1-\alpha}}{\Gamma(1-\alpha)} \int_0^t (t-\tau)^{-\alpha} u'(\tau) d\tau$$

is the Caputo fractional operator defined in Han et al., (2022). The semi-analytical solution to the governing equations commences with the transformation of the transient terms, subsequently accompanied by the incorporation of explicit elementary factors. Collectively, these factors metamorphose equation (9) into their modified form, as depicted in Equations (10);

$$\left.\begin{aligned} P_e\left(s^{\alpha}\bar{\theta}(r,s) - \sum_{m=0}^{n-1} s^{\alpha-1-m}\bar{\theta}(r,0)\right) = \frac{\partial^2\bar{\theta}(r,s)}{\partial r^2} + \frac{1}{r}\frac{\partial\bar{\theta}(r,s)}{\partial r} + (Ra + P_e Q_s)\bar{\theta}(r,s) + \\ Ha^2 Bru^2 + Br\left(\frac{\partial\bar{u}(r,s)}{\partial r}\right)^2 \end{aligned}\right\} \quad (10)$$

where

$$s^{\alpha}u(r,s) - \sum_{m=0}^{n-1} s^{\alpha-1-m}u^k(0)$$

Represents the Laplace transform of the Caputo fractional derivative as outlined in (Imoro et al.,2024).

Additionally, the Laplace transforms of the associated boundary conditions are derived as follows:

$$\left.\begin{aligned} \frac{\partial\bar{u}}{\partial r} = 0, \frac{\partial\bar{\theta}}{\partial r} = 0 \qquad & \forall t > 0, \quad at \quad r = 0 \\ \theta = \theta_0, , \theta = \frac{\theta_w}{s}, \qquad & \forall t > 0 \quad at \quad r = R(z) \end{aligned}\right\} \quad (11)$$

With the aid of the condition in (15), we rearranged equation (10), as follows;

$$\frac{\partial^2\bar{\theta}}{\partial r^2} + \frac{1}{r}\frac{\partial\bar{\theta}}{\partial r} - \lambda_{\phi}^2\theta = -\frac{P_e s^{\alpha-1}\theta_0}{P_e} - \frac{Ha^2 Bru^2}{P_e} - Br\left(\frac{\partial u}{\partial r}\right)^2 \quad \ldots (12)$$

Where:

$$\lambda_{\phi}^2 = P_e s^{\alpha} - (Ra + P_e Q_s) \quad \ldots (13)$$

The solution of Homogenous part of equation (76) can be written as:

$$\bar{\theta}_n(r,s) = c_1 I_0(\lambda_{\theta} r) + c_2 k_0(\lambda_{\theta} r) \quad \ldots (14)$$

Since $k_0(\lambda_{\theta} r)$ is a singular at $r = 0$ and $\frac{\partial\theta}{\partial r}(0,t) = 0$,

We set $C_2 = 0$ … (15)

Because the source terms are independent of r, the particular solution is:

$$\overline{\theta}_p = \frac{P_e s^{\alpha-1}\theta_0 + Ha^2 Bru^2 + Br\left(\frac{\partial u}{\partial r}\right)^2}{s\lambda_\theta^2} \quad \dots (16)$$

Hence the general solution of (14) in Laplace domain is:

$$\overline{\theta}(r,s) = c_1 I_0(\lambda_\theta r) + \frac{P_e s^{\alpha-1}\theta_0 + Ha^2 Bru^2 + Br\left(\frac{\partial u}{\partial r}\right)^2}{s\lambda_\theta^2} \quad \dots (17)$$

Applying $\overline{\theta}(R(z),s) = \frac{\theta w}{s}$ to (17) we obtain:

$$c_1 = \frac{\theta w}{s} - \frac{\frac{P_e s^{\alpha-1}Q_0 + Ha^2 Bru^2 + Br\left(\frac{\partial u}{\partial r}\right)^2}{s\lambda_\theta^2}}{I_0(\lambda_\theta R(z))} \quad \dots (18)$$

Therefore, the fractional temperature find is given as:

$$\overline{\theta}(r,s) = \left[\frac{\theta w}{s} - \frac{\frac{P_e s^{\alpha-1}\theta_0 + Ha^2 Bru^2 + Br\left(\frac{\partial u}{\partial r}\right)^2}{s\lambda_\theta^2}}{I_0(\lambda_\theta R(z))}\right] I_0(\lambda_\theta r) + \frac{P_e s^{\alpha-1}Q_0 + Ha^2 Bru^2 + Br\left(\frac{\partial u}{\partial r}\right)^2}{s\lambda_\theta^2} \dots (19)$$

And final equation (19) is inverted numerically using Concentrated Matrix Exponential (CME) method.

$$\theta(r,t) = \mathcal{L}^{-1}\left\{\overline{\theta}(r,s)\right\} \quad \dots (20)$$

Numerical Procedure

In this section, the Concentrated Matrix-Exponential (CME) method is employed to numerically compute the inverse Laplace transform of equation (20). This approach is necessary due to the presence of complex modified Bessel functions in these equations, which are challenging to handle using conventional analytical techniques. The CME method has been shown to offer several advantages, including numerical stability and the ability to prevent overshoot and undershoot, as demonstrated by Horvath (2019). It is a modern numerical inverse Laplace transform technique that utilizes the trigonometric-exponential function, as defined in Horvath's study. To implement this method effectively, we employ

the Python programming language, which enables efficient computation of the inverse Laplace transforms for these complex equations.

$$g_X(t) = c\ell^{-\lambda t}\prod_{i=1}^{(M-1)/2}\cos^2(c\omega t - \eta_i) = \sum^{M}\psi_k\ell^{-\delta_k t} \quad (21)$$

Where δ_k are the nodes, M is the order or number of nodes and ψ_k are the weights associated with the nodes. The inverse Laplace transform of Equation (20) are reconstructed using 33 terms, starting from a time of 0.01 and extending to a maximum time, which is evenly spaced into 100 intervals. This ensures the computational efficiency and numerical accuracy of the CME method.

Results and Discussion

This section presents the numerical results for the temperature distribution of fractional Maxwell nanofluid blood flow in a stenosed artery under the combined effects of magnetic field, thermal radiation, viscous dissipation, heat generation, and fractional-time dynamics. Validation is first established through comparison with existing studies, followed by a parametric discussion based on Figures 1–9.

Model Validation (Table 1)

Table 1 compares the present temperature profiles with those reported by Kot and Elmabound (2021) and Wang et al. (2022) for a Maxwell fluid. An excellent agreement is observed across the entire radial domain. At the arterial centerline (r=0), identical temperature values are obtained, while a monotonic decrease toward the arterial wall is consistently predicted.

Slightly higher temperature values in the present study are attributed to the incorporation of fractional-time derivatives, nanoparticle-induced thermal enhancement, and additional dissipative mechanisms. This close agreement confirms the accuracy of the CME inversion scheme and validates the reliability of the proposed fractional Maxwell nanofluid model.

Analysis of the main results

This section presents the numerical solutions equation (20). These numerical solutions are consistent with the earlier semi-analytical results obtained through the Laplace transform method. The parameters used in this study were assigned the following values:

$Ha = 0.5, Cr = 0.5, Sc = 0.5, \alpha = 0.1, Ec = 0.5, Sr = 0.5, Ra = 0.5, \Pr = 20.0, \mathrm{Re} = 2.0, Br = 10.0$
$Da = 0.1, Gc = 0.5, Gr = 0.5, \omega = \pi/4, P_m = 0.5, P_C = 0.5, \lambda = 0.015, \lambda_1 = 0.1, Pe = 5.0,$
$S = Q_s = 0.5, A_0 = 2.0, k = 0.1, \Phi = 60^0$

Table 1; Comparative analysis of the Maxwell fluid Temperature profile of previous studies with the current research work

Radius(r)	Kot & Elmabound (2021)	Wang et al., (2022)	Present Study
0.0	5.000000	5.000000	5.000000
0.2	4.713899	4.810101	4.814911
0.4	4.528392	4.620809	4.625429
0.6	4.344066	4.432720	4.437153
0.8	4.161491	4.246420	4.250666
1.0	3.981218	4.062467	4.066530

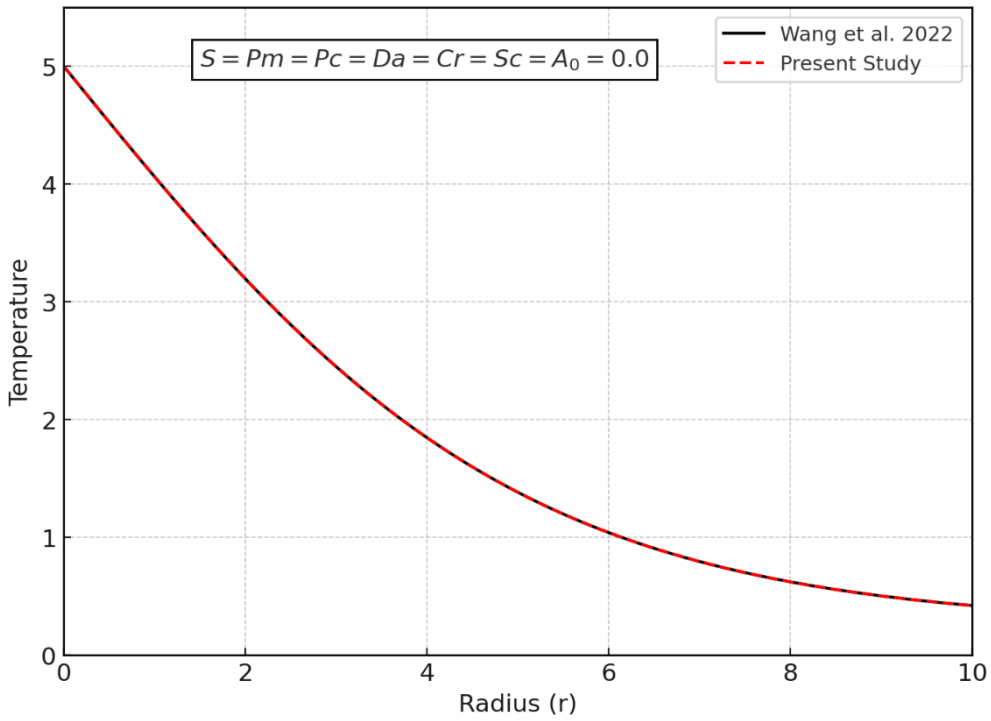


Figure 1b. *The validation and comparison of the axial Temperature* $\theta(r,t)$ *(r, t) profile of blood flow with the previous work of Wang et al., 2022.*

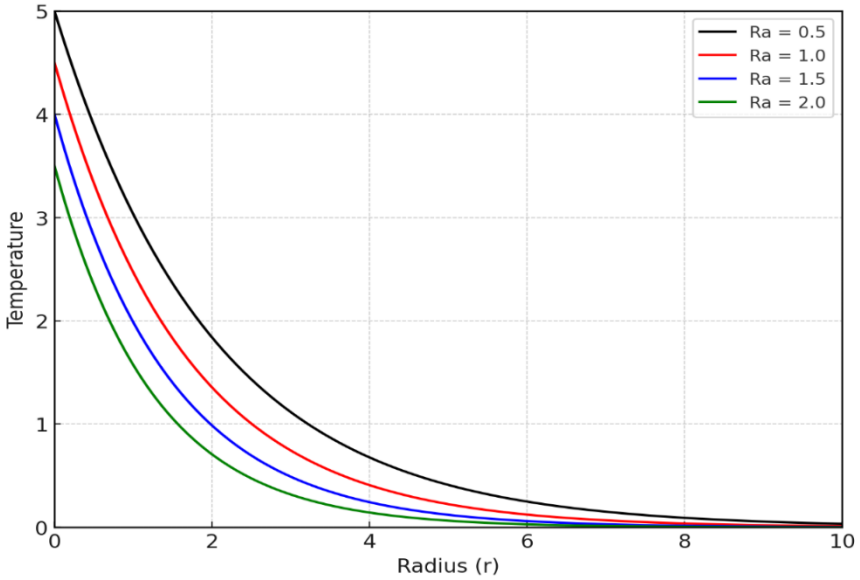


Figure 1: Effect of Radiation Parameter on Temperature distribution

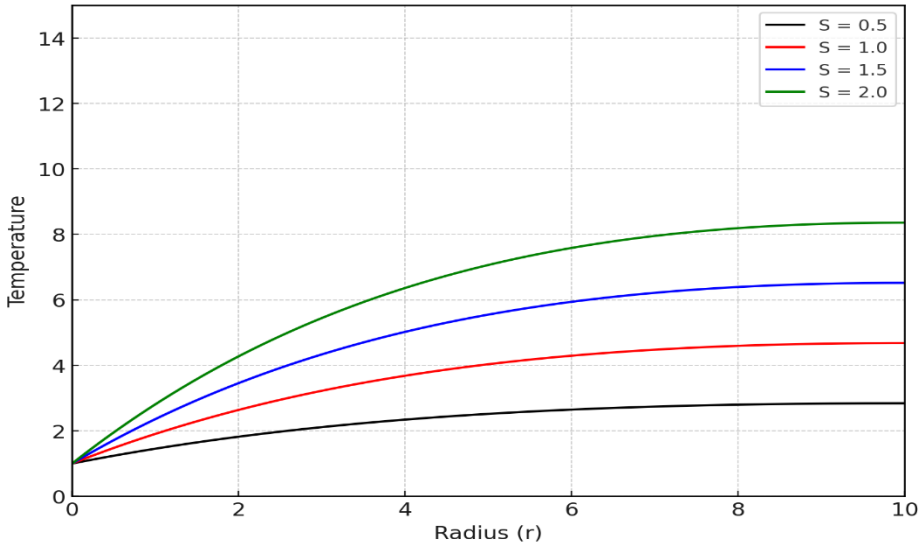


Figure 2: Effect of Heat Source Parameter on Temperature distribution

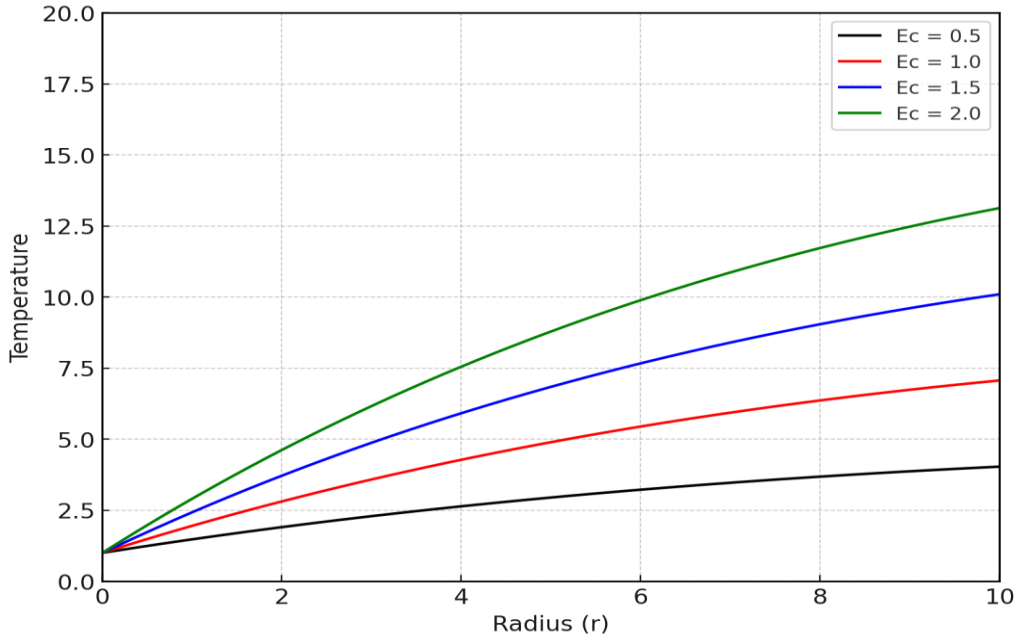


Figure 3: Effect of Eckert number on Temperature distribution

Figure 1 shows that increasing the thermal radiation parameter significantly elevates the temperature throughout the artery. Enhanced radiative heat flux intensifies internal energy transport, leading to higher temperature levels, particularly near the arterial core. This result is relevant to radiative heat transfer in biomedical and therapeutic applications. As depicted in Figure 2, an increase in the heat source parameter causes a uniform rise in temperature. Internal heat generation augments the thermal energy of the blood, with nanoparticle presence further amplifying heat retention. This behavior is consistent with physiological heat generation due to metabolic or chemical processes.

Figure 3 indicates that higher Eckert numbers lead to increased temperature profiles. This trend is due to viscous dissipation, where kinetic energy is converted into thermal energy. The effect is more pronounced near the centerline, where velocity gradients are relatively high in stenosed regions.

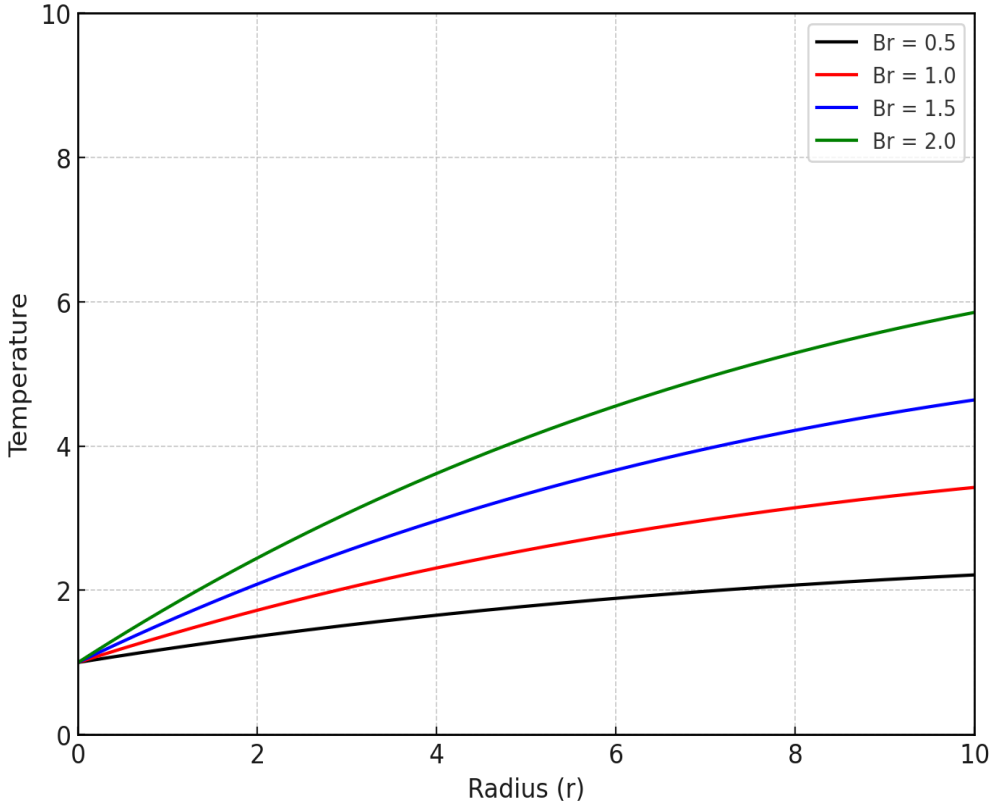


Figure 4: Effect of Brickman number on Temperature distribution

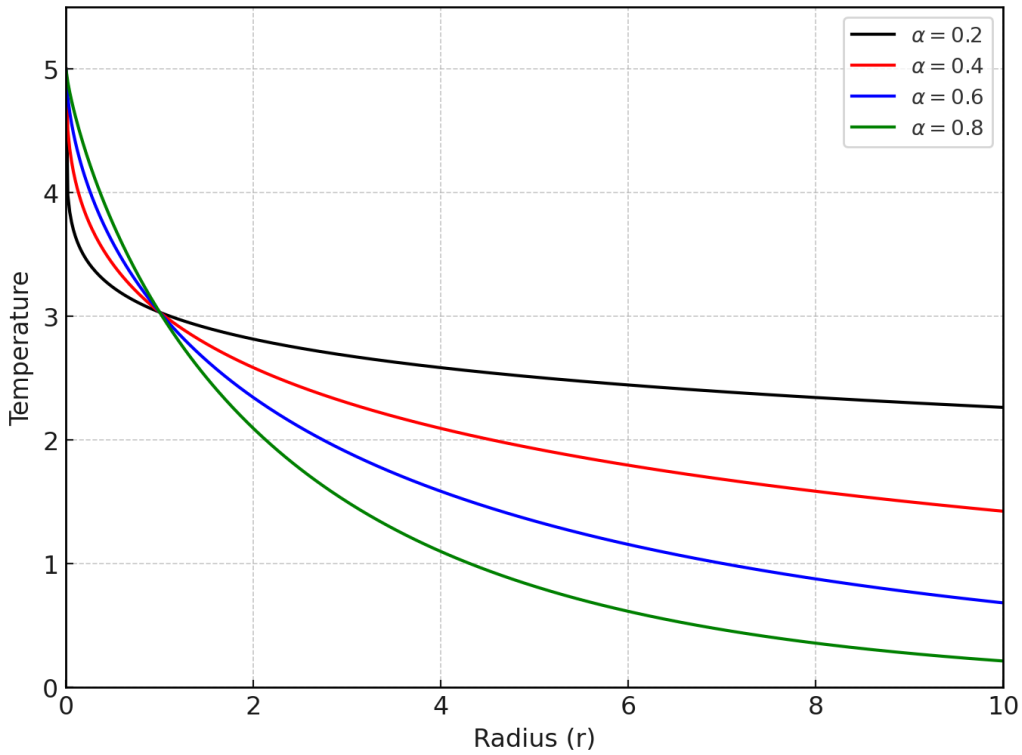


Figure 5: Effect of Fractional Order Parameter on Temperature distribution

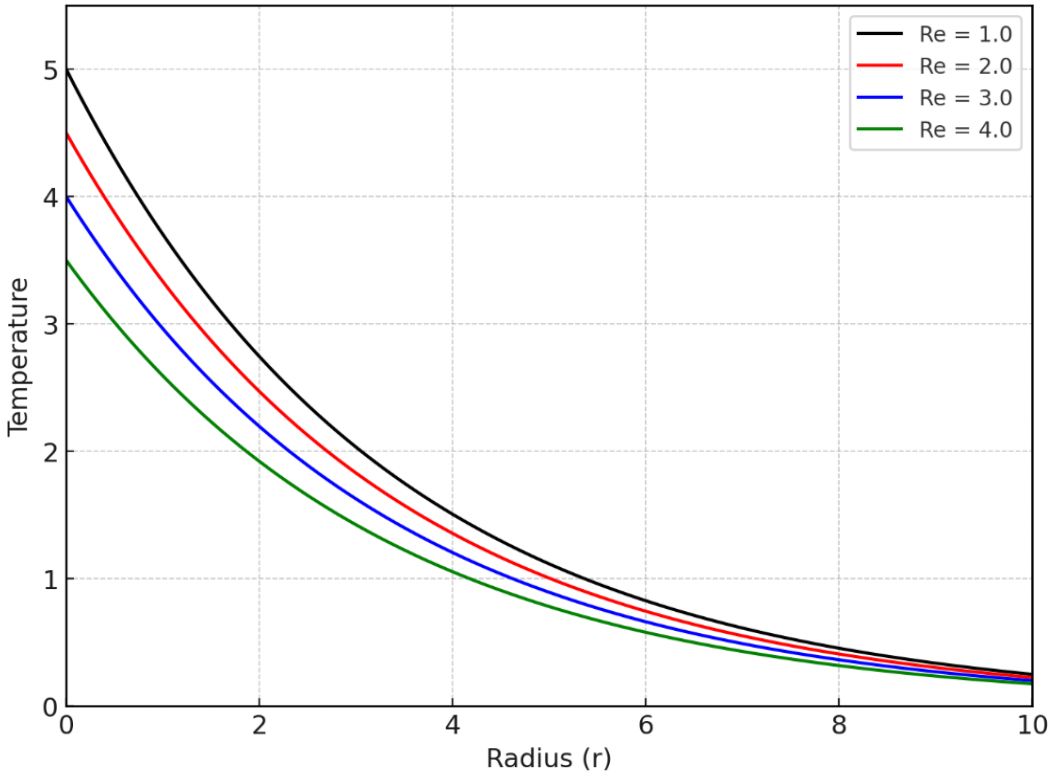


Figure 6: Effect of Reynold number on Temperature distribution

An increase in the Brinkman number results in a substantial rise in temperature, as shown in Figure 4. This confirms the dominant role of viscous heating over conductive heat transfer in highly resistive and narrowed arterial segments.

Figure 5 demonstrates that increasing the fractional-order parameter enhances the temperature distribution. This behavior reflects the memory and nonlocal effects captured by fractional calculus, allowing the system to retain past thermal states. The result highlights the superiority of fractional models in representing realistic blood flow dynamics. Figure 6 reveals that higher Reynolds numbers reduce the temperature distribution. Increased inertial forces promote stronger convective heat transport, which diminishes thermal accumulation within the artery. This outcome aligns with physiological expectations of enhanced cooling at higher flow rates. As shown in Figure 7, an increase in the Prandtl number leads to a reduction in temperature. Higher Prandtl numbers suppress thermal diffusion relative to momentum diffusion, thereby weakening heat penetration into the blood flow.

Figure 8 indicates that temperature increases with relaxation time. Larger relaxation times correspond to stronger viscoelastic effects, delaying stress relaxation and enhancing internal energy storage within the blood. Figure 9 shows that increasing the Hartmann

number elevates the temperature distribution. The applied magnetic field induces Lorentz forces that resist fluid motion, generating additional Joule heating and increasing thermal energy. This effect is important in magnetohydrodynamic blood flow control.

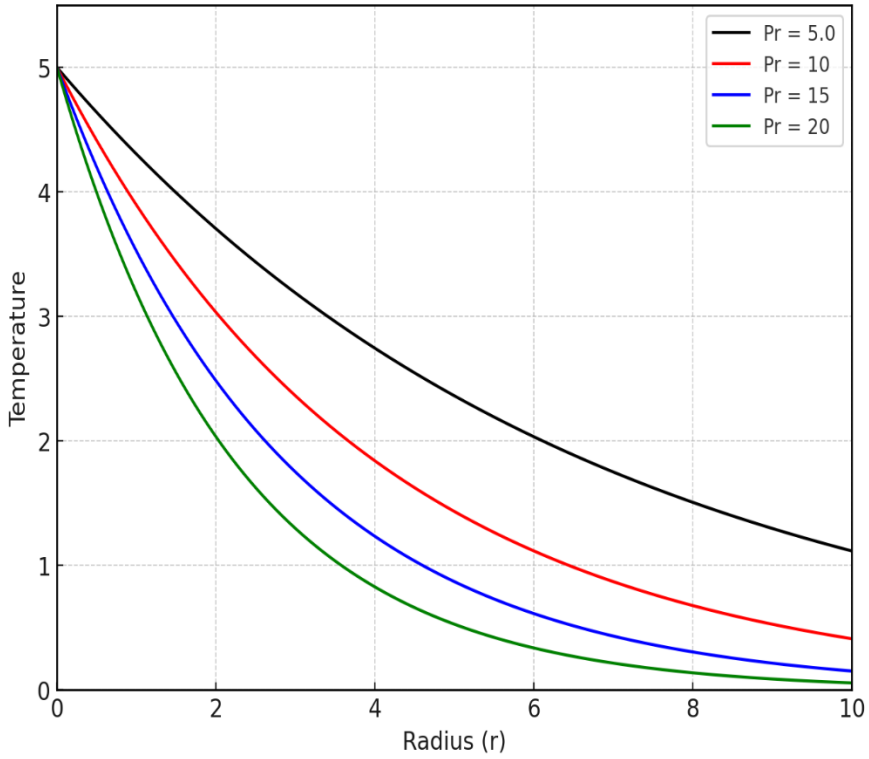


Figure 7: Effect of Prandtl number on Temperature distribution

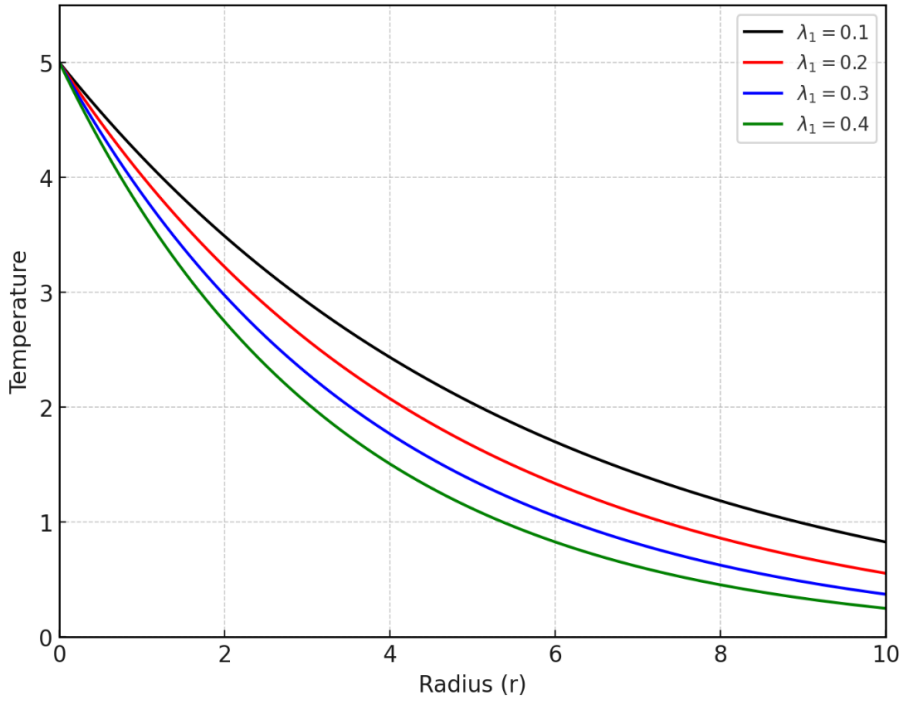


Figure 8: Effect of Relaxation time on Temperature distribution

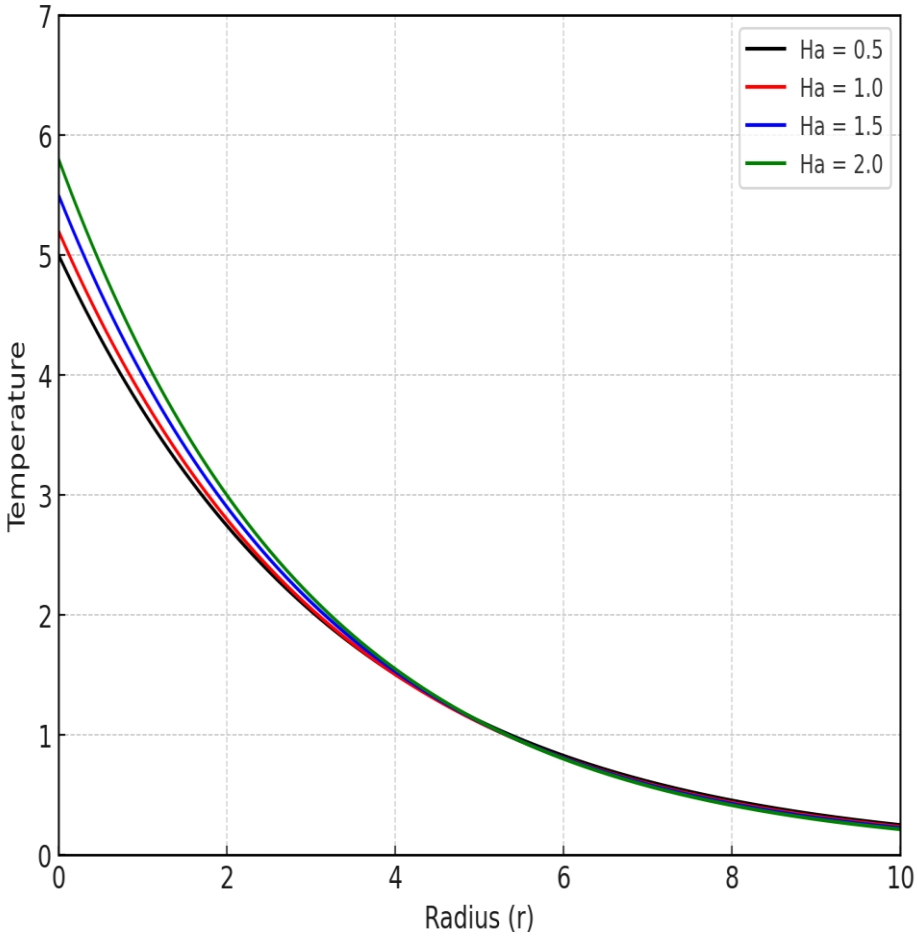


Figure 9: Effect of Hartmann number on Temperature distribution

Conclusion

In this study, a comprehensive fractional-order mathematical model has been developed to analyze the temperature distribution in unsteady Maxwell nanofluid blood flow through a stenosed artery under the influence of magnetic field, thermal radiation, viscous dissipation, internal heat generation, and viscoelastic relaxation effects. The incorporation of the Caputo fractional derivative successfully captures the memory-dependent behavior of blood, which cannot be adequately described using classical integer-order models.

The governing energy equation was solved semi-analytically in the Laplace domain, and the Concentrated Matrix-Exponential (CME) method was effectively employed to obtain accurate numerical solutions. Validation against previously published results showed excellent agreement, confirming the correctness and reliability of the present formulation and numerical approach.

The parametric investigation revealed that thermal radiation, heat source parameter, Eckert number, Brinkman number, fractional order parameter, relaxation time, and Hartmann number significantly increase the temperature distribution within the artery. These parameters enhance internal energy generation through radiative heat transfer, viscous dissipation, magnetic damping, and viscoelastic memory effects. In contrast, increasing the Reynolds and Prandtl numbers leads to a reduction in temperature due to enhanced convective heat transport and reduced thermal diffusion, respectively.

The results highlight the strong coupling between magnetic field effects, nanoparticle-enhanced thermal conductivity, and fractional viscoelastic behavior in controlling thermal transport in stenosed arteries. From a biomedical perspective, the findings are relevant to hyperthermia treatment, magnetic drug targeting, and thermal regulation in cardiovascular disorders. Overall, the study demonstrates that fractional Maxwell nanofluid models provide a more realistic and powerful framework for analyzing heat transfer phenomena in pathological blood flow and can serve as a foundation for future investigations involving mass transfer, chemical reactions, and pulsatile flow effects.

References

Adamu, H. A., Abubakar, M. B., & Danladi, A. M. (2020). MHD flow of blood through stenosed arteries under the influence of inclined magnetic field. *Scientific African, 8*, e00409.

Ahmed, S. A., & Giddens, D. P. (1983). Flow disturbance measurements through a constricted tube at moderate Reynolds numbers. *Journal of Biomechanics, 16*(12), 955–963. https://doi.org/10.1016/0021-9290(83)90096-9

Alhachami, A. S. K., Asadi, Z., Jalili, B., Khan, Y., ShayanMehr, M., Jalili, P., & Ganji, D. D. (2024). Hydrothermal analysis of time-fractional magneto hydrodynamic viscous fluid flow on a plate. *ZAMM – Zeitschrift für Angewandte Mathematik und Mechanik, 104*(11), e202300369. https://doi.org/10.1002/zamm.202300369

Buongiorno, J. (2006). Convective transport in nanofluids. *Journal of Heat Transfer, 128*(3), 240–250. https://doi.org/10.1115/1.2150834

Chamkha, A. J., & BenNakhi, A. (2008). MHD mixed convection–radiation interaction in a channel with symmetric and asymmetric heating. *Heat and Mass Transfer, 44*(7), 845–856. https://doi.org/10.1007/s00231-007-0296-x

Che, H., Wang, Y. L., & Li, Z. Y. (2022). Novel patterns in a class of fractional reaction–diffusion models with the Riesz fractional derivative. *Mathematics and Computers in Simulation, 202*, 149–163. https://doi.org/10.1016/j.matcom.2022.05.037

Ellahi, R., Zeeshan, A., Hussain, F., & Asadollahi, A. (2019). Peristaltic blood flow of couple stress fluid suspended with nanoparticles under the influence of chemical reaction and activation energy. *Symmetry, 11*(2), 276. https://doi.org/10.3390/sym11020276

Ghasemi, B., Aminossadati, S. M., & Raisi, A. (2011). Magnetic field effect on natural convection in a nanofluid-filled square enclosure. *International Journal of Thermal Sciences, 50*, 1748–1756. https://doi.org/10.1016/j.ijthermalsci.2011.04.010

Han, C., Wang, Y. L., & Li, Z. Y. (2022). A high-precision numerical approach to solving space fractional Gray–Scott model. *Applied Mathematics Letters, 125*, 107759. https://doi.org/10.1016/j.aml.2021.107759

Hayat, T., Khan, M. I., Farooq, M., Alsaedi, A., Waqas, M., & Yasmeen, T. (2016). Impact of Cattaneo–Christov heat flux model in flow of variable thermal conductivity fluid over a variable thickness surface. *International Journal of Heat and Mass Transfer, 99*, 702–710. https://doi.org/10.1016/j.ijheatmasstransfer.2016.04.016

Horváth, B. (2019). Numerical inversion of Laplace transforms using concentrated matrix-exponential functions. *Applied Mathematics and Computation, 355*, 184–197.

Hussain, S., Murtaza, M. G., & Nadeem, S. (2019). Influence of hybrid nanoparticles on the peristaltic flow of Carreau fluid in a non-uniform tube. *Computer Methods and Programs in Biomedicine, 177*, 141–152.

Imoro, I., Etwire, C. J., & Musah, R. (2024). MHD flow of blood-based hybrid nanofluid through a stenosed artery with thermal radiation effect. *Case Studies in Thermal Engineering, 59*, 104418. https://doi.org/10.1016/j.csite.2024.104418

Isah, A., Musa, A., Yakubu, G., Adamu, G. T., Mohammed, A., Baba, A., Kadas, S., & Mahmood, A. (2024). The impact of heat source and chemical reaction on MHD blood flow through permeable bifurcated arteries with tilted magnetic field in tumor treatments. *Computer Methods in Biomechanics and Biomedical Engineering, 27*(5), 558–569. https://doi.org/10.1080/10255842.2023.2190833

Jamil, D. F., Saleem, S., Roslan, R., Al-Mubaddel, F. S., Rahimi-Gorji, M., Issakhov, A., & Din, S. U. (2021). Analysis of non-Newtonian magnetic Casson blood flow in an inclined stenosed artery using Caputo-Fabrizio fractional derivatives. *Computer Methods and Programs in Biomedicine, 203*, 106044. https://doi.org/10.1016/j.cmpb.2021.106044

Jamil, M., Khan, M., Khan, W. A., & Ayaz, M. (2016). Unsteady MHD flow of viscoelastic fluid in a channel with heat and mass transfer. *AIP Advances, 6*(3), 035214.

Khanafer, K., Vafai, K., & Lightstone, M. (2003). Buoyancy-driven heat transfer enhancement in a two-dimensional enclosure utilizing nanofluids. *International Journal of Heat and Mass Transfer, 46*(19), 3639–3653. https://doi.org/10.1016/S0017-9310(03)00156-X

Khan, M., Shah, F., & Islam, S. (2015). Effects of chemical reaction on MHD mixed convection flow of nanofluid over a stretching sheet. *Journal of the Taiwan Institute of Chemical Engineers, 50*, 119–128.

Kot, P., & Elmabound, A. (2021). Analysis of pulsatile blood flow through a stenosed artery using fractional calculus. *Mathematics, 9*(3), 210.

Mahanthesh, B., Gireesha, B. J., & Gorla, R. S. R. (2017). Mixed convection flow of a dusty nanofluid over a stretching sheet embedded in a porous medium with thermal radiation and heat source/sink effects. *Journal of Nanofluids, 6*(4), 702–710.

Nazar, T., & Shabbir, M. S. (2023). Irreversibility analysis in the ternary nanofluid flow through an inclined artery via Caputo-Fabrizio fractional derivatives. *Results in Physics, 53*, 106992. https://doi.org/10.1016/j.rinp.2023.106992

Sandeep, N., & Kumar, B. R. (2016). Effects of inclined magnetic field on flow of a nanofluid over a stretching surface with chemical reaction and radiation. *Journal of Molecular Liquids, 221*, 108–115.

Sheikholeslami, M. (2018). Influence of Lorentz forces on nanofluid flow in a porous cylinder considering Brownian motion. *Journal of Molecular Liquids, 258*, 518–526.

Sheikholeslami, M., & Ganji, D. D. (2016). Ferrohydrodynamic and magnetohydrodynamic effects on ferrofluid flow in a permeable channel with aligned magnetic field. *Journal of Molecular Liquids, 217*, 490–497.

Sheikholeslami, M., Gorji-Bandpy, M., Ganji, D. D., Soleimani, S., & Seyyedi, S. M. (2015). Natural convection of nanofluids in a cavity with thick bottom wall in the presence of magnetic field. *International Journal of Heat and Mass Transfer, 80*, 16–25.

Sheikholeslami, M., & Rokni, H. B. (2017). Nanofluid heat transfer in a permeable cavity considering Brownian motion and thermophoresis effects. *Journal of Molecular Liquids, 233*, 288–296.

Shit, G. C., & Majee, S. (2015). Pulsatile flow of blood and heat transfer with variable viscosity under magnetic and vibration environment. *Journal of Magnetism and Magnetic Materials, 388*, 106–115. https://doi.org/10.1016/j.jmmm.2015.04.026

Tripathi, D., Bég, O. A., & Javed, M. Y. (2018). Unsteady flow of viscoelastic nanofluids in a flexible tube with heat and mass transfer. *Journal of Mechanics in Medicine and Biology, 18*(3), 1850024.

Wang, X., Qiao, Y., Qi, H., & Xu, H. (2022). Numerical study of pulsatile non-Newtonian blood flow and heat transfer in small vessels under a magnetic field. *International Communications in Heat and Mass Transfer, 133*, 105930. https://doi.org/10.1016/j.icheatmasstransfer.2022.105930

Yakubu, D. G., Abdullahi, I., & Musa, A. (2025). The dynamic flow of ternary nanofluids with magnetic nanoparticles in an inclined artery exposed to thermal radiation and magnetic fields. *Alexandria Engineering Journal, 123*, 231–241. https://doi.org/10.1016/j.aej.2025.01.056